THE JOURNAL OF BIOLOGICAL CHEMISTRY VOL. 291, NO. 32, pp. 16816–16827, August 5, 2016
© 2016 by The American Society for Biochemistry and Molecular Biology, Inc. Published in the U.S.A.

The Baseplate of *Lactobacillus delbrueckii* Bacteriophage Ld17 Harbors a Glycerophosphodiesterase*[S]

Received for publication, March 21, 2016, and in revised form, May 25, 2016 Published, JBC Papers in Press, June 6, 2016, DOI 10.1074/jbc.M116.728279

Anneleen Cornelissen[‡], Irina Sadovskaya[§], Evgeny Vinogradov[¶], Stéphanie Blangy[‖], Silvia Spinelli[‖**], Eoghan Casey[‡], Jennifer Mahony[‡], Jean-Paul Noben[‡‡], Fabio Dal Bello[§§], Christian Cambillau[‖**], and Douwe van Sinderen[‡¶¶1]**

*From the [‡]School of Microbiology and [¶¶]APC Microbiome Institute, University College Cork, Cork, Ireland, [§]Equipe Biochimie des Produits Aquatiques, Université du Littoral-Côte d'Opale, Boulevard du Bassin Napoléon, BP 120, 62327 Boulogne-sur-mer, France, [¶]National Research Council, 100 Sussex Drive, Ottawa K1A 0R6, Canada, [‖]Aix-Marseille Université, Architecture et Fonction des Macromolécules Biologiques, Campus de Luminy, 13288 Marseille Cedex 09, France, **CNRS, Architecture et Fonction des Macromolécules Biologiques, UMR 6098, Campus de Luminy, 13288 Marseille Cedex 09, France, [‡‡]Biomedical Research Institute (Biomed) and School of Life Sciences, Transnationale Universiteit Limburg, Hasselt University, Agoralaan-Building C, BE-3590 Diepenbeek, Belgium, and [§§]Sacco srl, 22071 Cadorago CO, Italy*

Glycerophosphodiester phosphodiesterases (GDPDs; EC 3.1.4.46) typically hydrolyze glycerophosphodiesters to *sn*-glycerol 3-phosphate (Gro3P) and their corresponding alcohol during patho/physiological processes in bacteria and eukaryotes. GDPD(-like) domains were identified in the structural particle of bacterial viruses (bacteriophages) specifically infecting Gram-positive bacteria. The GDPD of phage 17 (Ld17; $GDPD_{Ld17}$), representative of the group b *Lactobacillus delbrueckii* subsp. *bulgaricus* (Ldb)-infecting bacteriophages, was shown to hydrolyze, besides the simple glycerophosphodiester, two complex surface-associated carbohydrates of the Ldb17 cell envelope: the Gro3P decoration of the major surface polysaccharide D-galactan and the oligo(glycerol phosphate) backbone of the partially glycosylated cell wall teichoic acid, a minor Ldb17 cell envelope component. Degradation of cell wall teichoic acid occurs according to an exolytic mechanism, and Gro3P substitution is presumed to be inhibitory for $GDPD_{Ld17}$ activity. The presence of the $GDPD_{Ld17}$ homotrimer in the viral baseplate structure involved in phage-host interaction together with the dependence of native GDPD activity, adsorption, and efficiency of plating of Ca^{2+} ions supports a role for $GDPD_{Ld17}$ activity during phage adsorption and/or phage genome injection. In contrast to $GDPD_{Ld17}$, we could not identify any enzymatic activity for the GDPD-like domain in the neck passage structure of phage 340, a 936-type *Lactococcus lactis* subsp. *lactis* bacteriophage.

Glycerophosphodiester phosphodiesterases (GDPDs[2]; EC 3.1.4.46) are evolutionarily highly conserved proteins present in all domains of life (from bacteria to humans) (1). During degradation of the bacterial and eukaryotic cell membrane, the glycerophospholipid building blocks are first deacylated by phospholipases A_1 and A_2, resulting in the formation of glycerophosphodiesters. These glycerophosphodiesters, which differ based on the alcohol moiety present (*e.g.* choline, inositol, or glycerol), are further hydrolyzed by GDPDs, producing the corresponding alcohol and *sn*-glycerol 3-phosphate (Gro3P). GDPDs vary in their substrate specificity, biological function, and localization inside the cell. For bacteria, GDPDs, *e.g.* the well characterized *Escherichia coli* periplasmic GlpQ and cytosolic UgpQ, play an important role in glycerophospholipid metabolism where the released alcohol moiety may act as an essential bacterial growth factor and where the produced Gro3P represents a major carbon and phosphate source (2, 3). Some GDPDs are known to contribute to bacterial pathogenesis. For example, the *Haemophilus influenzae* GDPD, GlpQ, is a lipoprotein located in the outer membrane and contributes to bacterial pathogenesis through choline generation from the abundant pools of degradation products of the eukaryotic cell membrane. Consequent decoration of the *H. influenzae* cell wall with phosphorylcholine allows evasion from the host immune system through mimicry of the eukaryotic cell membrane (4). The canonical plant GDPD-encoding genes are upregulated by inorganic phosphate deprivation and have been shown to contribute to seedling growth (5) or root hair development and density (6). The seven different GDPD isoforms identified in humans display a high degree of substrate specificity (not necessarily a glycerophosphodiester) and tissue functionality. For example, human kidney GDE2 is an osmoregulated enzyme that controls the levels of the osmoprotector glycerophosphocholine (7), whereas it triggers motor neuron differentiation as part of the nervous system (8).

Interestingly, various genes that encode putative GDPDs have been identified in the genomes of bacteriophages infecting Gram-positive bacteria (*Clavibacter* phage CMP1 (9), *Staphy-*

* This work was supported by a Principal Investigator Awards 08/IN.1/B1909 and 13/IA/1953 (to D. v. S.) and an EMPOWER postdoctoral fellowship of the Irish Research Council (to A. C.). The authors declare that they have no conflicts of interest with the contents of this article.

[S] This article contains supplemental Figs. S1–S3 and Tables S1 and S2.

[1] To whom correspondence should be addressed: School of Microbiology and APC Microbiome Inst., University College Cork, Western Rd., Cork, Ireland. Tel.: 353-21-4901365; Fax: 353-21-4903101; E-mail: d.vansinderen@ucc.ie.

[2] The abbreviations used are: GDPD, glycerophosphodiester phosphodiesterase; Gro3P, *sn*-glycerol 3-phosphate; Ld, *L. delbrueckii*; Ldb, *L. delbrueckii* subsp. *bulgaricus*; CWTA, cell wall teichoic acid; NPS, neck passage structure; SEC-MALS-RI, size exclusion chromatography-multiangle light scattering-refractive index; GPC, glycerophosphorylcholine; HPAEC-PAD, high performance anion exchange chromatography with pulsed amperometric detection; CWaC, cell wall-associated carbohydrate; sPS, surface-associated polysaccharide; TA, teichoic acid; LTA, lipoteichoic acid.

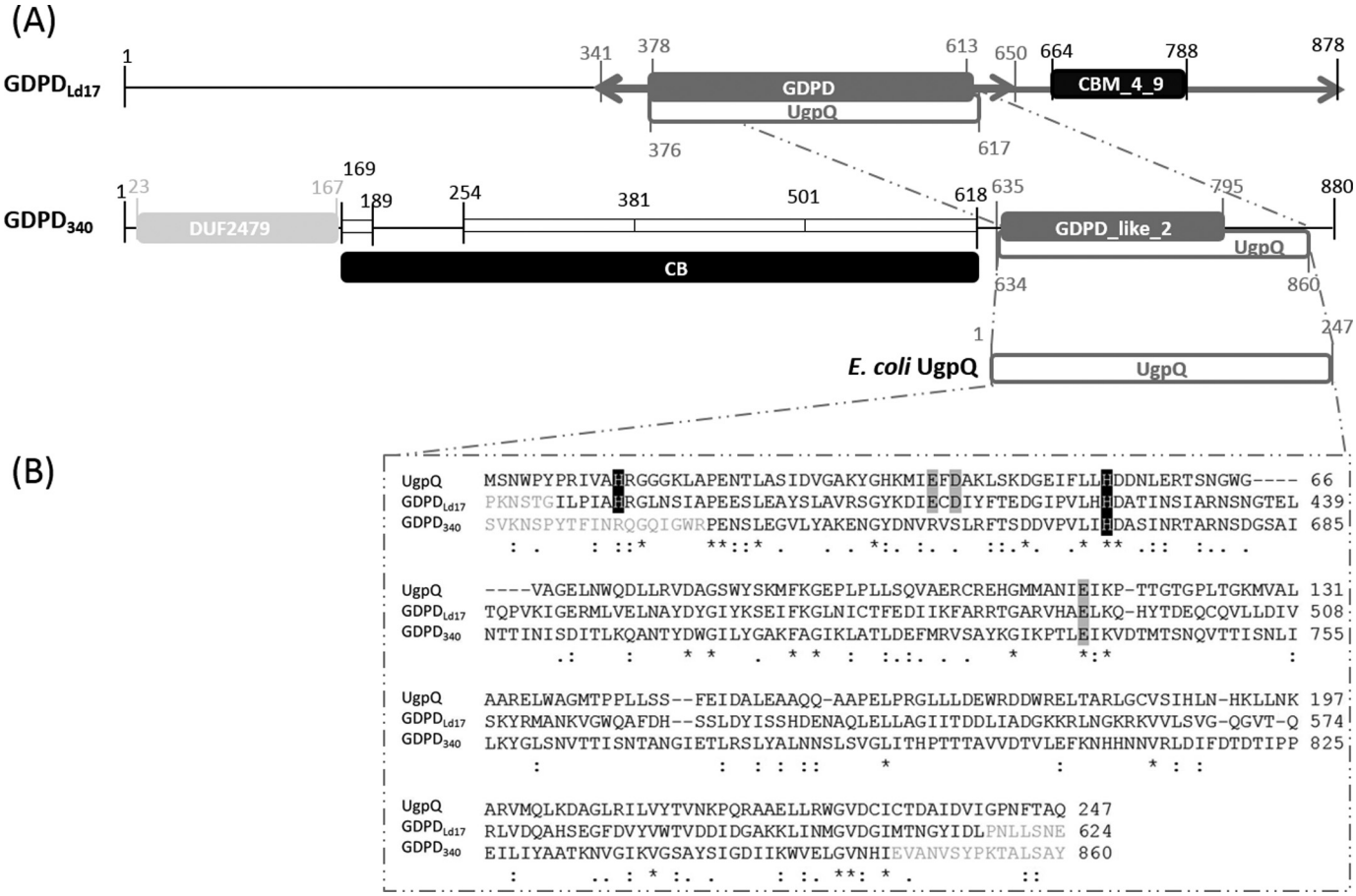

FIGURE 1. ***In silico* domain analysis of GDPD$_{Ld17}$ and GDPD$_{340}$.** *A*, modular structure of GDPD$_{Ld17}$ and GDPD$_{340}$ based on NCBI Conserved Domain Detection analysis (20). The predicted catalytic domains, GDPD (cd08556; 5.11E^{-38}) and GDPD_like_2 (cd08582; 7.40E^{-15}) are indicated as *dark gray boxes*. Sequence similarity (GDPD$_{Ld17}$, 9.86E^{-27}; GDPD340, 2.65E^{-09})) to the GDPD UgpQ of *E. coli* is depicted. The predicted carbohydrate-binding (*CB*) domain (CBM_4_9; 9.76E^{-03}) of GDPD$_{Ld17}$ and the putative carbohydrate-binding domain (residues 169–618) of GDPD$_{340}$ consisting of three ±124-amino acid repeating units and one partial repeating unit, as predicted by the Trust server (22), are indicated by *black boxes*. The extreme N-terminal domain of GDPD$_{340}$, probably involved in physical association with the virion, contains a DUF2479 domain (*light gray box*; 9.76E^{-03}), which is typically found in the neck passage structure of lactococcal 936-type phages. The *double arrows* delineate the "GDPD" and the "GDPD + CBM modules" of GDPD$_{Ld17}$ cloned and designated further as the "catalytic" and "catalytic + carbohydrate-binding" modules. *B*, ClustalW comparison of the UgpQ-like GDPD domains (amino acids in *light gray* were excluded from the NCBI Conserved Domain Detection delineation). The putative catalytic histidine residues are marked in *black*, and the glutamic acid and aspartic acid residues involved in binding of the divalent cations are marked in *dark gray*. Identical residues are marked by an *asterisk*, and residues marked with a *point* and *colon* display chemical and physical similarity, which is higher for the latter. Gaps, indicated by *horizontal lines*, were introduced into the sequences to maximize the alignment.

lococcus aureus phage K (10), and other "Twort"-like viruses (11–14), all group b *Lactobacillus delbrueckii* phages (15–17) and *Lactococcus lactis* subsp. *lactis* phages 340 and 645 (18, 19)). The bacteriophage GDPDs are encoded by the genomic region that is involved in virion morphogenesis. However, their predicted functionality has not yet been assessed.

The present study investigates the GDPD derived from the *L. delbrueckii* subsp. *bulgaricus* group b bacteriophage 17 (phage Ld17) and the *L. lactis* subsp. *lactis* bacteriophage 340 (phage 340) and represents the first characterization of bacteriophage-encoded GDPD. Besides an in-depth biochemical and molecular analysis of the GDPD of phage Ld17 (GDPD$_{Ld17}$), we studied substrate specificity and highlight the importance of the native GDPD$_{Ld17}$ during phage infection.

Results

The Presence of a GDPD Domain in Structural Phage Proteins with Distinct Topologies—The structural module of the genomes of all known group b *L. delbrueckii*-infecting phages and of the *L. lactis* subsp. *lactis*-infecting phages 340 and 645 contains a gene that encodes a protein containing a GDPD(-like) domain. Because of the high protein identity of these putative GDPD-containing proteins within the group b Ldb-infecting phages (93–95% identity) and between the two *L. lactis* ssp. *lactis*-infecting phages (phages 340 and 645; 99% identity), the GDPDs of phage Ld17 (designated here as GDPD$_{Ld17}$) and 340 (named GDPD$_{340}$) were selected as representatives of the respective phage groups.

Bioinformatics analysis revealed an apparent tripartite domain structure in both GDPDs (Fig. 1*A*): (i) an N-terminal domain that is presumably required for physical association with the phage particle, (ii) a putative carbohydrate-binding domain, and (iii) the GDPD(-like) domain with the latter two domains displaying an inverse arrangement in GDPD$_{Ld17}$ and GDPD$_{340}$. NCBI Conserved Domain Detection analysis (20) identified a DUF2479 domain (residues 23–167; 9.76E^{-03}) within the N terminus of GDPD$_{340}$; this domain is a typical feature of the neck passage structure (NPS) of lactococcal 936-

type phages to which phage 340 belongs (21). Transmission electron micrographs of immunogold-labeled $GDPD_{340}$ confirm the presence of $GDPD_{340}$ as part of the phage 340 NPS (Fig. 2*B*). No conserved domains were detected in the N terminus of $GDPD_{Ld17}$, whereas immuno-EM using anti-$GDPD_{Ld17}$ antibodies revealed that the GDPD protein of Ld17 is associated with the baseplate of phage Ld17 (Fig. 2*A*).

Although a conserved carbohydrate-binding domain (CBM_4_9; residues 664–788; $9.76E^{-03}$) is present in the C terminus of $GDPD_{Ld17}$, we hypothesize that a carbohydrate-binding function is present in the central domain of $GDPD_{340}$ based on the identification of a ±124-amino acid repeating unit using the Trust server (22). The full repeat region (residues 169–618) consisting of three full repeating units of ±124 amino acids and one partial unit suggests interaction with a (repeated) component of the bacterial cell envelope and is therefore assigned as the putative carbohydrate-binding domain of $GDPD_{340}$.

Sequence similarity between $GDPD_{Ld17}$ and $GDPD_{340}$ is restricted to their GDPD(-like) domains, which share 28 and 20% amino acid identity, respectively, with the well characterized cytoplasmic *E. coli* protein UgpQ. The GDPD domain (residues 378–613) of $GDPD_{Ld17}$ belongs to the large family of the canonical prokaryotic and eukaryotic GDPDs (EC 3.1.4.46) represented by UgpQ. ClustalW alignment (Fig. 1*B*) highlights in the GDPD-domain of $GDPD_{Ld17}$ the presence of five conserved amino acid residues, two catalytic histidine residues (His-381 and His-421 in $GDPD_{Ld17}$) and three residues (Glu-408, Asp-410, and Glu-491) for binding a divalent cation, which are believed to be involved in the catalytic metal ion-dependent acid-base reaction mechanism to hydrolyze glycerophosphodiester linkages (23). The GDPD-like domain (residues 635–795) of $GDPD_{340}$ belongs to a subfamily of uncharacterized bacterial GDPDs (cd08582; $7.40E^{-15}$); curiously, ClustalW alignment identified just two (His-669 and Glu-737) of the five conserved residues that are associated with the typical GDPD-mediated reaction mechanism.

Structural Characteristics—Consistent with the immunogold electron microscopy findings (Fig. 2), mass spectrometric analyses of Ld17 (17) and 340 (supplemental Table S2) virions indicates the presence of the full-length GDPDs as part of the structural phage particle. Full-length $GDPD_{Ld17}$ and $GDPD_{340}$ were recombinantly expressed and purified using the *L. lactis* NZ9000-pTX8048 expression system (24). Mass calculations using SEC-MALS-RI analyses of the purified recombinant $GDPD_{Ld17}$ and $GDPD_{340}$ proteins revealed the presence of complexes with estimated masses of 325 and 326 kDa, respectively, which correspond to the homotrimeric native conformations (theoretical molecular masses of 111.9 and 110.7 kDa for $GDPD_{Ld17}$ and $GDPD_{340}$ monomers, respectively) (Fig. 3*A*). Moreover, $GDPD_{Ld17}$ appears to form a sodium dodecyl sulfate (SDS)-resistant homotrimer at room temperature (Fig. 3*B*). An estimated molecular mass of ~335 kDa, consistent with a homotrimer, was observed when unheated samples of $GDPD_{Ld17}$ were loaded on a 7% (w/v) SDS-polyacrylamide gel, whereas a band consistent with the theoretical molecular mass of the monomer (111.9 kDa) was observed when the protein sample was boiled for 5 min prior to loading on the SDS-polyacrylamide gel. The $GDPD_{340}$ protein does not display this SDS resistance characteristic at room temperature and appears to disassemble

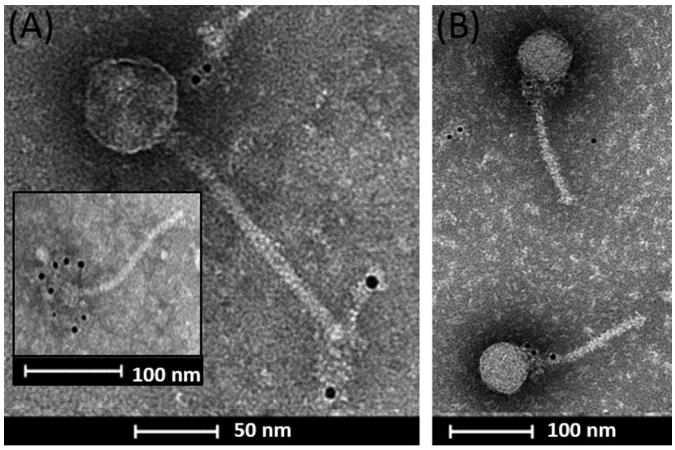

FIGURE 2. **Transmission electron micrographs of immunogold-labeled GDPD protein as part of the baseplate of *L. delbreuckii* subsp. *bulgaricus* phage 17 (*A*) and as part of the neck passage structure of *L. lactis* subsp. *lactis* phage 340 (*B*).** Phages were incubated with polyclonal anti-GDPD rabbit antibodies raised against the GDPD specific for that phage and labeled with anti-rabbit secondary mouse antibodies conjugated to 5-nm gold particles.

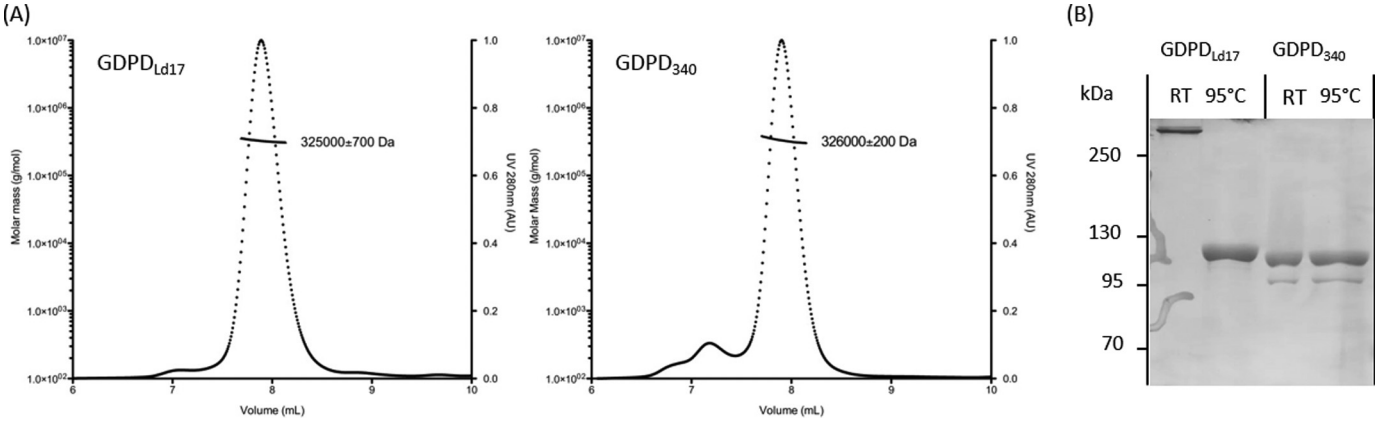

FIGURE 3. **$GDPD_{Ld17}$ and $GDPD_{340}$ are trimeric proteins.** *A*, SEC-MALS-RI chromatogram of the $GDPD_{Ld17}$ (111.9-kDa theoretical molecular mass; *left*) and $GDPD_{340}$ (110.7-kDa theoretical molecular mass; *right*). The molar mass (*left axis*, *solid line*) and the $UV_{280\ nm}$ absorbance (*right axis*, *dotted line*) are plotted as a function of the column elution volume. *B*, protein bands of $GDPD_{Ld17}$ and $GDPD_{340}$ on a 7% (w/v) SDS-polyacrylamide gel with (95 °C, 5 min) and without (room temperature (*RT*), 5 min) boiling prior to electrophoresis. *AU*, arbitrary units.

TABLE 1

Enzymatic activity of $GDPD_{Ld17}$ on purified carbohydrates

GDPD activity expressed as $\Delta A_{340\ nm}$/(μmol of GDPD × min) was evaluated using an enzyme-coupled spectrophotometric assay on 1.5 g/liter purified carbohydrates. Average and S.D. of three repeats are given. HPAEC-PAD chromatograms of purified carbohydrates (2.5 g/liter) exposed to $GDPD_{Ld17}$ at 30 °C for 2 h detected only Gro3P as the end product of $GDPD_{Ld17}$ activity.

	Chemical structure	Ref.	GDPD activity	HPAEC-PAD
			$\Delta A_{340\ nm}$/ ($\mu mol \times min$)	
Cell wall teichoic acid				
S. aureus NM8m	*N*-Acetyl-D-glucosaminated poly(ribitol phosphate) D-alanylated poly(glycerol phosphate)	29	137.33 ± 1.33	Gro3P
S. epidermidis 1457	D-Alanylated, D-glucosylated, *N*-acetyl-D-glucosaminated poly(glycerol phosphate)	This study	172.44 ± 5.05	Gro3P
S. epidermidis RP62A	D-Alanylated, D-glucosylated (partially D-alanylated at C6), *N*-acetyl-D-glucosaminated poly(glycerol phosphate)	28	11.11 ± 0.77	Gro3P
L. delbrueckii subsp. *bulgaricus* 17	D-Alanylated, D-glucosylated oligo(glycerol phosphate) units	27	31.56 ± 0.77	Gro3P
B. subtilis 168	D-Alanylated, D-glucosylated poly(glycerol phosphate)	30	56.67 ± 3.45	Gro3P
B. subtilis W23	D-Alanylated, D-glucosylated poly(ribitol phosphate)	31	3.20 ± 0.79	
Extracellular teichoic acid				
L. monocytogenes ScottA			5.33 ± 1.33	
Lipoteichoic acid				
S. aureus (Sigma-Aldrich)			5.33 ± 1.33	
B. subtilis (Sigma-Aldrich)			6.66 ± 1.33	
L. lactis subsp. *cremoris* MG1363			5.33 ± 2.31	
Cell wall-associated polysaccharide				
L. lactis subsp. *cremoris* MG1363, pellicle	Hexasaccharide repeating units linked by phosphodiester bonds	26	2.22 ± 2.04	
L. delbrueckii subsp. *bulgaricus* 17, sPS1	Neutral branched hexasaccharide repeating units	27	3.33 ± 1.92	
L. delbrueckii subsp. *bulgaricus* 17, sPS2	Glycerol 3-phosphorylated linear D-galactan	27	873.33 ± 13.33	Gro3P
L-α-Glycerophosphorylcholine		70	2753.33 ± 34.64	Gro3P

into its monomers with or without a heating step prior to or upon electrophoresis.

Enzymatic Activity and Substrate Preference of $GDPD_{Ld17}$—During metabolism or pathogenesis, bacterial GDPDs are known to hydrolyze deacylated phospholipids, called glycerophosphodiesters, into the corresponding alcohol and Gro3P. Therefore, we analyzed in the first instance the ability of the bacteriophage-encoded GDPDs to degrade glycerophosphorylcholine (GPC), a glycerophosphodiester, with HPAEC-PAD analysis in parallel with an enzyme-coupled spectrophotometric assay quantifying the formation of Gro3P. The specific GDPD activity of $GDPD_{Ld17}$, expressed as $\Delta A_{340\ nm}$/(μmol of GDPD × min) using 2.5 mM GPC substrate after 30-min incubation at 30 °C was 7466.67 ± 108.44 (supplemental Fig. S1A). In parallel, the HPAEC-PAD chromatogram showed one additional peak at 42 min after $GDPD_{Ld17}$ treatment of the GPC substrate that we attribute to the formation of Gro3P (data not shown).

As the bacterial GDPDs perform a second step in cell membrane degradation subsequent to deacetylation of the glycerophospholipids by phospholipase A, we presumed that these glycerophosphodiesters are not the natural substrates of the bacteriophage-encoded GDPD but that this activity is serendipitous. Because bacteriophage-encoded GDPDs, which are a structural component of the virion, are most likely to interact with phosphodiester-containing substrates (*e.g.* teichoic acids (25) or other surface-associated carbohydrates (26)) in the host cell envelope, we implemented an extraction procedure to concentrate cell wall-associated carbohydrates (CWaCs) excluding peptidoglycan.

HPAEC-PAD analysis of the CWaC extract of Ldb17, the bacterial host of phage Ld17, displayed an extra peak at 42 min following $GDPD_{Ld17}$ treatment compared with the negative buffer control (data not shown). This peak corresponds to the Gro3P peak liberated in the presence of the GPC substrate. Using an enzyme-coupled spectrophotometric assay specific for the detection of Gro3P, the $GDPD_{Ld17}$ activity on the Ldb17 CWaC extract was quantified as 2071.11 ± 37.91 $\Delta A_{340\ nm}$/(μmol of GDPD × min). These results imply the presence of carbohydrate substrates in the Ldb17 cell envelope that, following $GDPD_{Ld17}$ hydrolysis, generate a reaction product identical to that generated during GPC hydrolysis, namely Gro3P.

We have recently identified two carbohydrates associated with the Ldb17 cell surface that contain Gro3P: a Gro3P-substituted linear D-galactan, surface-associated polysaccharide 2 (sPS2), with the following repeating unit (-(Gro-3*P*-(1–6)-)-3-β-Gal*f*-3-α-Gal*p*-2-β-Gal*f*-6-β-Gal*f*-3-β-Gal*p*-) and short chain cell wall teichoic acid (CWTA) structures with a partially glycosylated poly(glycerol phosphate) backbone (27). Using an enzyme-coupled spectrophotometric assay, a $GDPD_{Ld17}$ activity of 31.56 ± 0.77 and 873.33 ± 13.33 $\Delta A_{340\ nm}$/(μmol of GDPD × min) was identified on the CWTA and the Gro3P-decorated D-galactan of Ldb17, respectively (Table 1). NMR analysis of $GDPD_{Ld17}$-treated sPS2 showed the absence of all signals of Gro3P (Fig. 4). Although native sPS2 contained ~0.7 μM/mg of phosphate, the phosphate content of the $GDPD_{Ld17}$-treated sPS2 was below the level of detection. HPAEC-PAD (Table 1) further confirmed the cleavage of Gro3P from these purified carbohydrates after exposure to $GDPD_{Ld17}$.

To gain further insight into the substrate specificity of $GDPD_{Ld17}$, a spectrum of purified carbohydrates after treatment with $GDPD_{Ld17}$ (in parallel with a buffer control) was analyzed with HPAEC-PAD. According to HPAEC-PAD anal-

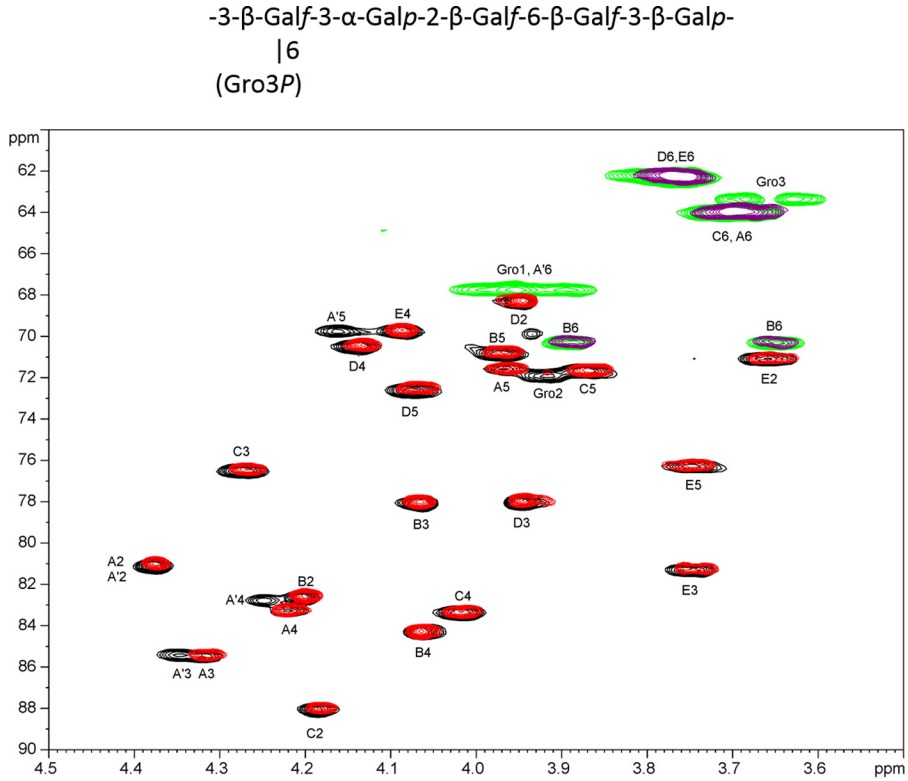

FIGURE 4. **NMR analysis of the GDPD$_{Ld17}$-treated Gro3P-substituted linear D-galactan (sPS2) of Ldb17.** Chemical structure (27) and part of the heteronuclear single quantum coherence spectrum of the Ldb17 sPS2 (*green-black*) and GDPD$_{Ld17}$-treated Ldb17 sPS2 (*red-violet*). Note the absence of Gro and A′ signals in the GDPD$_{Ld17}$-treated sPS2 spectrum.

yses (Table 1), the sole end product of GDPD$_{Ld17}$ hydrolysis is Gro3P, which is removed from the poly(glycerol phosphate) CWTA backbone, the Gro3P-decorated linear D-galactan, and the bacterial GPC. The single Gro3P peak observed in the HPAEC-PAD chromatograms of all poly(glycerol phosphate) CWTA exposed to GDPD$_{Ld17}$ at any time point in the incubation when measuring GDPD$_{Ld17}$ activity in the linear activity range or when excess GDPD$_{Ld17}$ protein (10-fold the amount compared with the highest amount used in the linear range of activity) is applied during longer incubation periods (up to 2 h) suggests exolytic activity for GDPD$_{Ld17}$ whereby Gro3P units are released one by one from the CWTA ends. Furthermore, the absence of peaks other than that corresponding to Gro3P and the correlation between the observed Gro3P peak volume in the HPAEC-PAD chromatograms and the Gro3P quantification by an enzyme-coupled spectrophotometric assay suggests that decorated, typically by glycosylation or D-alanylation for CWTA, Gro3P units in the CWTA backbone are not removed. This indicates that GDPD$_{Ld17}$-mediated degradation of CWTA is terminated at a substituted Gro3P unit. This notion is consistent with the low GDPD$_{Ld17}$ activity (11.11 ± 0.77) observed for *Staphylococcus epidermidis* RP62A CWTA (28), which has a higher degree of substitution compared with *S. aureus* NM8m (29) (137.33 ± 1.33) and *Bacillus subtilis* 168 (30) (56.67 ± 3.45) (Table 1). Gel filtration chromatography of the long poly(glycerol phosphate) CWTA of two *S. epidermidis* strains, 1457 and 5, also confirms exolytic cleavage of unsubstituted Gro3P units by GDPD$_{Ld17}$. The purified CWTAs of 1457 and 5 are in the size range of about 10 kDa consisting of 30–50 Gro3P units. The relative molar ratio (glycerol:glucose:*N*-acetylglucosamine) of 1457 and 5 CWTAs was assessed as 15:1:1.5 and 50:1:1.8, respectively. Because of this glycosylation combined with partial D-alanylation of the poly(glycerol phosphate) backbone, the number of unsubstituted Gro3P units cleaved off from the CWTA end is restricted, resulting in the absence of smaller oligo(glycerol phosphates) during gel filtration of 1457 and 5 CWTAs treated with excess GDPD$_{Ld17}$ for 2 h at 30 °C (supplemental Fig. S2). Other phosphodiester bonds, *i.e.* those that connect hexasaccharide repeats in the lactococcal pellicle of MG1363 (26) or those present in the poly(ribitol phosphate) TA of *B. subtilis* W23 (31), are insensitive to GDPD$_{Ld17}$ hydrolysis, thus indicating a requirement for glycerol adjacent to the phosphodiester bond (Table 1). However, lipoteichoic acid (LTA) is not degraded by GDPD$_{Ld17}$ despite the fact that CWTA and LTA share a similar 1→3 poly(glycerol phosphate) backbone. It should be noted that CWTA possesses a Gro3P repeating unit, whereas the repeating unit (and thus the unit available for GDPD$_{Ld17}$ at the end) of the LTA backbone is *sn*-glycerol 1-phosphate, which has an opposite stereochemistry on C2 of the glycerol unit compared with Gro3P. The absence of any degradation in the HPAEC-PAD chromatogram of purified LTAs following GDPD$_{Ld17}$ treatment indicates a strict preference for the Gro3P configuration.

Biochemical and Structural Requirements for GDPD$_{Ld17}$ Activity—The optimal biochemical characteristics for GDPD$_{Ld17}$ activity were assayed on Ld17 CWaC extract (3 μg/μl) in the linear range of enzymatic activity using an enzyme-coupled

spectrophotometric assay (supplemental Fig. S3). The highest $GDPD_{Ld17}$ activity is observed in the temperature range of 30–42 °C at pH 8 in the presence of 10 mM Ca^{2+}. Although Mg^{2+} gradually inhibits $GDPD_{Ld17}$ activity upon increasing concentration with 25% relative activity at 100 mM $MgCl_2$, other divalent cations (Mn^{2+}, Co^{2+}, Ni^{2+}, Cd^{2+}, and Zn^{2+}) display a stronger inhibitory effect with complete absence of enzymatic activity at 5 mM.

Because most bacterial GDPDs in the NCBI database are of similar size (30–40 kDa) as the GDPD domain of $GDPD_{Ld17}$, the individual central GDPD domain alone (48.8 kDa) or this domain in combination with the putative carbohydrate-binding domain (73.8 kDa) was recombinantly expressed using the pTX8048 lactococcal expression vector, and their enzymatic activity was evaluated using an enzyme-coupled spectrophotometric assay on the Ldb17 CWaC extract and GPC. Both truncated derivatives had lost more than 98% activity in comparison to the full-length $GDPD_{Ld17}$ protein (supplemental Fig. S1A) as well as the ability to form homotrimers resistant to SDS at room temperature (supplemental Fig. S1B). As trimerization of the truncated proteins was not analyzed by size exclusion chromatography, one may argue that the ability to form homotrimers was already lost upon truncation. Nevertheless, loss of (SDS-resistant) trimerization upon truncation and near complete loss of enzymatic activity of the truncated domains indicate the involvement of the deleted regions in both processes. Individual site-directed mutagenesis of each of the five conserved residues (His-381, Glu-408, Asp-410, His-423, and Glu-491; Fig. 1*B*) of $GDPD_{Ld17}$ putatively involved in a typical GDPD-reaction mechanism reduced the total activity to below 3%, both on the GPC substrate and on the (assumed) native substrate (Ld17 CWaC-extract) for each of the five generated mutant proteins. SDS-PAGE without prior boiling of the protein sample indicates that these five mutagenized proteins are still able to form SDS-resistant homotrimers (supplemental Fig. S1B), implying no major conformational changes of the mutagenized proteins and affirming the involvement of the five conserved residues within $GDPD_{Ld17}$ in the hydrolysis of the typical glycerophosphodiester and of the native Ld17 carbohydrates.

Absence of Detectable Enzymatic Activity for $GDPD_{340}$—The HPAEC-PAD chromatograms did not show any activity of $GDPD_{340}$ on GPC and on CWaC-extracts of the phage 340 host, IL1403, or of other lactococcal and *Lactobacillus* strains (data not shown). Also an enzyme-coupled spectrophotometric assay with higher sensitivity than HPAEC-PAD for Gro3P detection could not detect any GDPD activity. This absence of enzymatic activity for $GDPD_{340}$ suggests that this protein does not possess GDPD activity, which may have been caused by mutations that altered three of the five conserved residues implicated in the GDPD catalytic reaction mechanism (Fig. 1*B*).

GDPD Activity and Phage Ld17 Characteristics—The cation Ca^{2+} is essential for enzymatic activity of the recombinantly expressed $GDPD_{Ld17}$, whereas other divalent cations inhibit enzymatic activity (see above). To evaluate the importance of the native GDPD activity in the baseplate of the Ld17 virion for the phage infection process, different phage characteristics (native GDPD activity, adsorption, and efficiency of plating) were assessed in the presence of a diverse set of 20 mM divalent cations (Table 2). Similar to the recombinantly expressed $GDPD_{Ld17}$, the native GDPD activity of the Ld17 virion is stimulated by the addition of Ca^{2+} ions (relative activity of 127%), whereas the other divalent cations have an inhibitory effect. Mg^{2+} is again the less potent inhibitor with 33% activity remaining compared with the complete absence of GDPD activity after addition of any other inhibiting divalent cation. In parallel with the GDPD activity, the adsorption and the relative efficiency of plating of phage Ld17 on the host Ldb17 are optimal with values of 91% and 1.00, respectively, in the presence of 20 mM $CaCl_2$. Adsorption and plaque formation are less efficient in the presence of the other inhibiting divalent cations with only 71% adsorption and a relative efficiency of plating of 0.57 for Mg^{2+}.

Further evaluation of the enzymatic activity of the recombinantly expressed $GDPD_{Ld17}$ on CWaC extracts of a diverse set of 12 *L. delbrueckii* subsp. *bulgaricus* strains (Table 3), six sensitive (Ldb9, -10, -2, -14, -41, and -40) and six resistant (Ldb17, -36, -22, -34, -35, and -66) for phage Ld17 infection (17), indicates that all strains have carbohydrate structures associated with the cell envelope sensitive for GDPD activity. Furthermore, the variation within the GDPD activity is independent of the phage Ld17 sensitivity of the *L. delbrueckii* host.

TABLE 2

Influence of 20 mM divalent cations on phage Ld17 characteristics

The native GDPD activity present in the Ld17 virion was assayed in 50 mM MOPS (pH 7.5), 300 mM NaCl on 2.5 mM GPC substrate after incubation at 30 °C for 2 h with the enzyme-coupled spectrophotometric assay. 100% activity is set equal to the condition without additional divalent cations. Adsorption of phage Ld17 on its host Ldb17 is expressed as the ratio of adsorbed phage after 10 min to the number of free phages at time point 0. The relative efficiency of plating (EOP) of phage Ld17 on its host Ldb17 was compared with the optimal condition containing 20 mM $CaCl_2$. Relative efficiency of plating was not determined (ND) for Cd^{2+} and Zn^{2+} due to the absence of bacterial growth of the Ldb17 host under these conditions. For each condition, the average and S.D. of three independent experiments is given.

	Relative activity	Adsorption	Relative EOP
	%	%	
None	100.0 ± 1.0	75.7 ± 3.8	0.00 ± 0.00
Ca^{2+}	127.2 ± 2.0	91.0 ± 0.2	1.00 ± 0.16
Mg^{2+}	32.8 ± 1.1	71.1 ± 4.9	0.57 ± 0.04
Mn^{2+}	0.2 ± 0.2	64.6 ± 1.8	0.40 ± 0.03
Co^{2+}	0.0 ± 0.9	44.8 ± 3.6	0.00 ± 0.00
Ni^{2+}	0.0 ± 0.2	64.7 ± 6.2	0.00 ± 0.00
Cd^{2+}	0.0 ± 0.2	48.6 ± 6.1	ND
Zn^{2+}	0.0 ± 0.2	75.7 ± 3.8	ND

TABLE 3

Enzymatic activity of $GDPD_{Ld17}$ on a diverse set of CWaC extracts

GDPD activity expressed as $\Delta A_{340\ nm}/(\mu mol\ of\ GDPD \times min)$ was evaluated using an enzyme-coupled spectrophotometric assay on 1.5 g/liter CWaC extracts. Average and S.D. of three repeats are given.

L. delbrueckii subsp. *bulgaricus* strains	GDPD activity
	$\Delta A_{340\ nm}/(\mu mol \times min)$
Ldb9	697.78 ± 7.70
Ldb10	1402.22 ± 13.88
Ldb2	480.00 ± 6.67
Ldb14	1522.22 ± 15.40
Ldb41	873.33 ± 6.67
Ldb40	337.78 ± 16.78
Ldb17	962.22 ± 10.18
Ldb36	508.89 ± 34.21
Ldb22	328.89 ± 25.24
Ldb34	1024.44 ± 20.37
Ldb35	860.00 ± 61.10
Ldb66	504.44 ± 27.76

Discussion

The GDPD of bacteriophage Ld17 displays the characteristics of the canonical GDPD activity as identified in the literature (1): enzymatic activity requires (i) a divalent cation(s) and (ii) a conserved set of five amino acids for a metal ion-dependent, acid-base reaction mechanism to hydrolyze a (iii) glycerophosphodiester substrate to Gro3P and an alcohol. $GDPD_{Ld17}$ solely requires Ca^{2+} for activity, whereas other divalent cations are inhibitory for activity. This is probably a reflection of an adaptation to the high Ca^{2+} levels present in the dairy environment from which the Ld17 phage was isolated (17). Also the optimal temperature range (30–42 °C) for activity reflects the preferred growth conditions of the *Lactobacillus* host. Besides degradation of the simple glycerophosphodiester GPC, $GDPD_{Ld17}$ also elicits activity toward more complex substrates, the Gro3P decoration of the Ld17 D-galactan polysaccharide and the poly(glycerol phosphate) backbone of CWTA, in all cases releasing Gro3P. Degradation of CWTA occurs according to an exolytic mechanism, and substitution of the CWTA backbone is presumed to be inhibitory for $GDPD_{Ld17}$ activity. Although GDPD hydrolysis of more complex substrates has not been identified before for the canonical GDPDs, the $GDPD_{Ld17}$ activity is still in congruence with the recognition of the glycerophospho moiety by the canonical GDPDs and the formation of Gro3P end product (23, 32): the three conserved residues (Glu, Asp, and Glu) in the catalytic groove coordinate a divalent cation, which stabilizes the cyclic phosphate intermediate formed by glycerol and phosphate during a two-step reaction mechanism with the two catalytic histidine residues acting as a general acid and base. The involvement of the glycerol unit in the catalytic reaction mechanism explains the absence of any hydrolyzing activity by $GDPD_{Ld17}$ on carbohydrates with phosphodiester bonds not adjacent to a glycerol unit, such as the *L. lactis* MG1363 pellicle and poly(ribitol phosphate) TA. Moreover, the reaction mechanism is specific for *sn*-glycerol 3-phosphate, the repeat unit of the CWTA backbone, whereas the stereoisomer *sn*-glycerol 1-phosphate, the repeat unit of the poly(glycerol phosphate) backbone of lipoteichoic acid, is not recognized by $GDPD_{Ld17}$.

CWTA degradation by bacterial enzymes has so far only been described in, now vintage, research articles by Kusser and Fiedler (33–35). During sporulation, *B. subtilis* strain Marburg produces a TA-degrading enzyme with absolute substrate specificity for the endogenous α-glucosylated glycerol TA of the cell, producing the α-D-glucose 1→2 (*sn*)glycerol 3-phosphate according to an exolytic mechanism (33, 34). Phosphate-starved *Bacillus pumilus* DSM27 cells produce a TA-degrading enzyme that produces Gro3P using unsubstituted TA of the poly(glycerol phosphate) type as substrate, whereas the enzyme is unable to remove substituted glycerol phosphate (46). Although both bacterial TA-degrading enzymes display GDPD-like activity, the question remains whether the canonical bacterial GDPDs also display this teichoic acid-degrading activity. Further research of the bacterial GDPD substrate specificity is, as such, required.

Immuno-EM analysis showed that $GDPD_{Ld17}$ is part of the baseplate of phage Ld17. $GDPD_{Ld17}$ activity removes the Gro3P decoration of the D-galactan polysaccharide, the major charged carbohydrate associated with the Ldb17 cell wall, and can further degrade the short chain partially glycosylated oligo(glycerol phosphate) CWTA, which is a minor cell envelope component (27). Within bacteriophages, a very diverse set of enzymatic activities within baseplate-associated proteins, tail spikes, or fibers that interact with a component of or are closely associated with the bacterial cell envelope have been identified. These virion-associated enzymes (partially and locally) degrade the (corresponding) bacterial cell envelope component to accomplish accessibility to the underlying primary bacterial receptor to which the bacteriophage will irreversibly adsorb. To this group belong structural enzymes degrading lipopolysaccharide (36–38), exopolysaccharide (39–41), and capsule (42–44) structures and a small set of capsule deacetylases (45, 46). Furthermore, peptidoglycan-degrading enzymes associated with the tail tip of the virion ensure injection of the phage genomic DNA into the bacterial cell (47–51). Within the baseplate-encoding region of phage Ld17, no peptidoglycan-degrading activity was predicted, and because the carbohydrate substrates of $GDPD_{Ld17}$ are newly identified, it is difficult to infer whether GDPD activity of phage Ldb17 is involved in rendering accessibility to the bacterial receptor and/or injection of the phage genomic DNA into the cytosol. Moreover, the Ca^{2+} requirement for optimal $GDPD_{Ld17}$ activity and for efficient phage Ld17 adsorption and plaque formation suggests a general adaptation of the enzymatic activities of phage Ldb17 and the different steps of its infection cycle to a Ca^{2+}-rich environment or a dependence of adsorption and/or genomic DNA injection on $GDPD_{Ldb17}$ activity, resulting in a more efficient infection cycle.

L. delbrueckii subsp. *bulgaricus* is a commonly used in starter cultures in the commercial production of fermented milk products (yogurts and cheeses) where it contributes to the flavor profile of the final product (52). Infection of starter cultures during dairy fermentation by bacteriophages may disable (part of) the starter culture, thereby negatively influencing the fermentation process and the organoleptic characteristics of the dairy product. Despite its industrial significance, only one specific bacteriophage-host interaction between a *L. delbrueckii* strain, ATCC 15808, and its infecting phage, the group a *L. delbrueckii* phage LL-H, has been studied in depth (53–56). However, group b *L. delbrueckii*-infecting phages represent the most important genotype infecting *L. delbrueckii* (17). All group b *L. delbrueckii*-infecting phages possess a structural GDPD that shows 93–95% amino acid identity to $GDPD_{Ld17}$, and all have a full set of the conserved five amino acids involved in the canonical GDPD activity. Also all tested CWaC extracts of *L. delbrueckii* subsp. *bulgaricus* strains were shown to be highly sensitive for GDPD activity (Table 3). The absence of any detectable LTA and only limited amounts of CWTA (27), which is susceptible to GDPD hydrolysis, further suggest bacteriophage adsorption to a cell wall component different from TA, whereas most bacteriophages infecting Gram-positive bacteria (*e.g. Staphylococcus* species (57, 58), *B. subtilis* (59–61), *Listeria monocytogenes* (62, 63), and the group a *L. delbrueckii* phage LL-H (64) adsorb to TA structures. As such, further research unraveling the precise role of the GDPD during the infection process of group b *L. delbrueckii* phages will provide

us with new insights for strategies to prevent lysis of starter cultures during dairy fermentation.

We were not able to identify any enzymatic activity for $GDPD_{340}$. In comparison with the canonical GDPDs, $GDPD_{340}$ seems to have lost three of the five amino acid residues essential for canonical GDPD activity. $GDPD_{340}$ is part of the NPS of phage 340, a 936-type phage. The lactococcal 936-type phages are a well studied phage group because of their importance for the dairy industry, often (negatively) influencing dairy fermentation processes. The "older" 936-type phage isolates have no NPS (*e.g.* sk1 and p2) or a truncated NPS without any enzymatic domain (*e.g.* bIL140 and P008). More recent phage isolates from the dairy environment frequently possess a large NPS with a potential enzymatic domain, a GDPD-like domain (phages 340 and 645; Refs. 18 and 19), or an SNGH hydrolase domain (21, 65, 66). These "novel" enzymatic activities within the 936-type NPS are probably beneficial, but not essential, for bacteriophage infection in the dairy environment. It therefore appears that such enzymatic activity merely constitutes an accessory function that can be lost without loss of phage viability as can be hypothesized for $GDPD_{340}$. Nonetheless, $GDPD_{340}$ may conversely represent a non-canonical GDPD with activity different from the typical hydrolysis of glycerophosphodiesters, and the reaction conditions used in this study may have been unsuitable for detection of this enzymatic activity. For example, the mammalian GDE4 and GDE7 degrade glycerolysolipids (1), the GDPD of *Mycoplasma hyorhinis* displays, besides a typical GDPD activity, also nonspecific phospholipase A activity (68). Furthermore, Simocková *et al.* (69) identified phospholipase C activity that controls the phosphatidylglycerol content of the cell membranes in the bioinformatically annotated GDPD-like protein Pgc1p of *Saccharomyces cerevisiae*.

Experimental Procedures

Bacterial Strains, Bacteriophages, and Growth Conditions—*L. delbrueckii* subsp. *bulgaricus* strains were grown at 42 °C in MRS broth (Oxoid, UK) supplemented with 1% (w/v) lactose, 20 mM $CaCl_2$, and 0.5% (w/v) tryptone. *E. coli* strain MC1000 was grown aerobically at 37 °C in lysogeny broth. *L. monocytogenes* strains were kindly provided by Prof. M. J. Loessner (Institute of Food, Nutrition and Health, ETH Zurich, Switzerland) (62) and cultivated aerobically in brain heart infusion medium (Oxoid) at 30 °C. *L. lactis* subsp. *lactis* strain IL1403, the propagation host of phage 340, and *L. lactis* subsp. *cremoris* NZ9000, the host strain for protein (over)expression, were cultured in GM17 broth, M17 broth (Oxoid) supplemented with 0.5% (w/v) D-glucose under static conditions at 30 °C. *L. lactis* subsp. *cremoris* NZ9000 transformants were selected on GM17 agar plates with 5 μg/ml chloramphenicol (Sigma-Aldrich).

Propagation of *L. delbrueckii* subsp. *bulgaricus* phage 17 (Ld17) (17) on its host Ldb17 and *L. lactis* phage 340 (19) on IL1403 was initiated by infecting a liquid culture (2% inoculum of the host) with $\pm 10^6$ plaque-forming units (pfu)/ml at an $A_{600\,nm}$ of 0.150 and 0.600, respectively. Cultures were incubated at the incubation temperature of the host until complete lysis was observed. After addition of 0.5 M NaCl, bacterial debris was removed by centrifugation (8,700 × *g*, 15 min). Phages were precipitated from the supernatant with 10% (w/v) polyethylene glycol 8000 (PEG_{8000}; 8,700 × *g*, 15 min) and resuspended in phage buffer (20 mM Tris-HCl (pH 7.5) buffer supplemented with 10 mM $MgSO_4$, 300 mM NaCl, and 50 mM $CaCl_2$). Residual PEG_{8000} was removed by chloroform extraction (1:1). The resulting clarified phage suspension was layered on a CsCl step gradient (1.33, 1.50, and 1.70 g/cm^3), centrifuged at 104,333 × *g* for 3 h at 4 °C. The extracted phage band was finally dialyzed against phage buffer using Slide-A-Lyzer dialysis cassettes (Pierce) and stored at 4 °C.

Adsorption Assays—A 1-ml sample was taken of a bacterial suspension grown to midexponential phase ($A_{600\,nm}$ of 0.550; $\pm 5 \times 10^7$ CFU/ml) and centrifuged (15,000 × *g*, 10 min). The bacterial pellet was resuspended in 900 μl of MRS broth supplemented with 1% (w/v) lactose, 0.5% (w/v) tryptone, and a 20 mM concentration of the relevant divalent cations prewarmed at 42 °C. 100 μl of 5×10^5 pfu phages were added to generate a final multiplicity of infection of 0.02. Following incubation at 42 °C for 10 min, the bacterial host cells (including irreversibly adsorbed phages) were removed by centrifugation (15,000 × *g*, 7 min). The supernatant was titrated using the double agar overlay method with MRS soft and solid agar supplemented with 20 mM $CaCl_2$ to determine the number of non-adsorbed or reversibly adsorbed phages.

Analysis of Structural Phage 340 Proteins—The structural proteins of the *L. lactis*-infecting phage 340 were extracted from a CsCl-purified phage suspension (10^{10} pfu) using the methanol/chloroform (1:1:0.75, v/v/v) extraction protocol described by Moak and Molineux (48). The resulting protein pellet was resuspended in an SDS-PAGE loading buffer, boiled for 10 min, and loaded onto a standard 12% polyacrylamide gel (71). The structural proteome lane on the polyacrylamide gel was cut into slices that were individually subjected to trypsin digestion and peptide extraction according to Lavigne *et al.* (72). The collected peptides were analyzed by electrospray ionization-MS/MS.

Cloning of GDPD and Derivatives—Purified bacteriophage genomic DNA served as template for amplification of the coding regions (of the truncated derivatives) of the (putative) glycerophosphodiester phosphodiesterase-encoding genes using the KOD high fidelity DNA polymerase (Novagen, UK) and specific primer pairs (Eurofins MWG, Germany) (supplemental Table S1). Phage genomic template DNA was prepared by infecting *L. lactis* subsp. *lactis* IL1403 and *L. delbrueckii* subsp. *bulgaricus* 17 at an $A_{600\,nm}$ of 0.15 with 340 and Ld17, respectively, followed by incubation until lysis was observed. The resulting lysate was passed through a 0.45-μm filter (Sarstedt, Germany) followed by total genomic DNA extraction (73). PCR products were digested with BamHI (Roche Applied Science) and XbaI (Roche Applied Science), cloned into the similarly digested expression vector pTX8048 (24), and finally ligated using T4 DNA ligase (Promega). Ligation mixtures of PCR fragments and pTX8048 were introduced into *L. lactis* subsp. *cremoris* NZ9000 by electroporation, and resulting transformants were selected on GM17 agar plates supplemented with 5 μg/ml chloramphenicol. The generated constructs were verified by DNA sequencing using vector-specific and internal sequencing primers (supplemental Table S1).

Site-directed Mutagenesis of Amino Acid Residues Involved in the Catalytic Reaction Mechanism—Site-directed mutagenesis was performed by PCR using the template plasmid pTX8048-*gdpd* and the respective primer couples Ld17_XxxxAf and Ld17_XxxxAr (the catalytic residue, *X*, on position xxx of the protein sequence was replaced by an alanine residue, Ala) (supplemental Table S1). The "overhang" primers consist of 11 nucleotides 5′ of the mutated triplet and 27 nucleotides 3′. The template DNA was extracted using a GeneJET Plasmid Miniprep kit (Thermo Scientific) from dam$^+$ *E. coli* MC1000 to ensure its methylation. PCR amplification was performed in 50-μl volumes with ~10 ng of template, 1 unit of KOD Hot Start DNA polymerase (EMD Chemicals, Gibbstown, NJ), 1× KOD Hot Start DNA polymerase buffer, 200 μM dNTPs, 1.5 mM $MgSO_4$, and a 0.5 μM concentration of the respective primers. Cycling conditions consisted of an initial polymerase activation (95 °C, 2 min) followed by 95 °C for 20 s, 60 °C for 10 s, and 70 °C for 3 min for 35 cycles followed by a final extension for 7 min. PCR-generated amplicons were purified using the GeneJET PCR Purification kit (Thermo Scientific) followed by DpnI treatment (Stratagene) at 37 °C for 3 h to restrict all methylated template plasmid. After a final purification (GeneJET PCR Purification kit), the mutated pTX8048-*gdpd* was transformed into electrocompetent *L. lactis* subsp. *cremoris* NZ9000 and selected for on GM17-Cm^5 agar plates. After plasmid extraction, the mutations were verified by DNA sequencing using vector-specific and internal sequencing primers (supplemental Table S1).

Recombinant Protein Expression and Purification—Protein expression using the nisin-inducible expression system of pTX8048 provides an N-terminal protein fusion to thioredoxin to improve protein solubility and to a His_6 tag for protein purification purposes (25). Expression occurred at 30 °C for 3 h in *L. lactis* subsp. *cremoris* NZ9000 in GM17 broth supplemented with 5 μg/ml chloramphenicol after induction at an $A_{600\ nm}$ of 0.20 with 40 ng/ml nisin using Nisaplin powder (2.5% nisin; Danisco, UK) dissolved in sterile water. Cells were harvested from suspension by centrifugation (8,700 × *g*, 10 min, 4 °C). The bacterial pellet was washed once in lysis buffer (10 mM Tris-HCl (pH 7.5), 0.3 M NaCl, 10 mM $CaCl_2$) and finally stored overnight at −20 °C.

The bacterial pellet was thawed at room temperature, resuspended in lysis buffer (10 mM Tris-HCl (pH 7.5), 0.3 M NaCl, 10 mM $CaCl_2$) supplemented with 30 mg/ml hen egg white lysozyme (Sigma-Aldrich), and incubated at 20 °C for 30 min. The bacterial suspension was subsequently placed on ice and disrupted with glass beads in a Mini Bead Beater (Biospec Products, Bartlesville, OK) for 90 s followed by 5 min on ice for three cycles. Cell debris and insoluble components were discarded by centrifugation (25,000 × *g*, 30 min, 4 °C). Purification of the recombinant N-terminal His_6-tagged proteins was performed using the nickel-nitrilotriacetic acid-agarose (Qiagen, UK) according to the manufacturer's protocol with the wash and elution buffers composed of 10 mM Tris-HCl (pH 7.5), 0.3 M NaCl, 10 mM $CaCl_2$ supplemented with 20 and 150 mM imidazole, respectively.

Protein purity was at least 95% as estimated by SDS-PAGE. Protein concentration was estimated by the Bradford assay (74). Purified protein was dialyzed overnight against a volume of buffer at least 1000× the volume of the protein sample using Slide-A-Lyzer® MINI dialysis units (Pierce).

SEC-MALS-RI Analysis—Size exclusion chromatography of recombinantly purified GDPDs was performed on an Alliance HPLC 2695 system (Waters) using a 15-ml KW803 column (Shodex) and a phosphate-based saline buffer system (137 mM NaCl, 2.7 mM KCl, 10 mM Na_2HPO_4, 2 mM KH_2PO_4 (pH 7.2)) at a flow rate of 0.5 ml/min. MALS, UV spectrophotometry, quasielastic light scattering, and RI analyses were executed with a MiniDawn Treos (Wyatt Technology), Photo Diode Array 2996 (Waters), DynaPro (Wyatt Technology), and Optilab rEX (Wyatt technology), respectively (75). The mass and hydrodynamic radius were calculated with the ASTRA software (Wyatt Technology) using a d*n*/d*c* value of 0.185 ml/g.

Immunoelectron Microscopy—Purified phage preparation was dialyzed for 15 min against TGB buffer (200 mM Tris-HCl (pH 7.5), 500 mM glycine, 2% (v/v) butanol) using a Novagen D-Tube™ dialyzer (molecular mass cutoff, 3.5 kDa). Dialyzed phages were put over a nickel glow-discharged grid for 30 min and incubated overnight (20 °C) with primary antibody solution diluted 1:90 in TGB buffer. The grid was washed then in TGB buffer and incubated for 1 h in a 1:40 dilution of the secondary antibody solution (goat anti-rabbit immunoglobulin G 5-nm gold conjugate solution). Fixation was achieved using 0.25% (v/v) glutaraldehyde for 20 min in phosphate-based saline buffer at room temperature. The grid was washed and blotted five times in filtered dialyzed water. Finally, the samples were stained with 2% phosphotungstic acid (pH 7.0) for about 30 s and observed using a Tecnai Spirit electron microscope operated at 120 kV and a 2,000 × 2,000-pixel charge-coupled device camera. Polyclonal antibodies against the recombinantly purified $GDPD_{Ld17}$ and $GDPD_{340}$ were raised in rabbits by Davids Biotechnologie GmbH (Regensburg, Germany).

Extraction of Cell Wall-associated Carbohydrates—A culture flask of 800 ml of fresh medium was inoculated with a 1% bacterial overnight culture and grown overnight (±20 h) at the appropriate temperature. Cells were harvested by centrifugation (8,700 × *g*, 15 min) and washed three times in 20 mM $NH_4C_2H_3O_2$·AcOH (pH 4.7). The bacterial pellet was resuspended in 20 mM $NH_4C_2H_3O_2$·AcOH (pH 4.7) supplemented with 4% SDS and boiled in a water bath with intensive stirring for 1.5 h. After cooling the bacterial suspension to room temperature, the bacterial cells were collected by centrifugation (8,700 × *g*, 15 min), and the cell pellet was washed three to five times with 20 mM $NH_4C_2H_3O_2$·AcOH (pH 4.7) until no SDS-mediated foaming was observed. The pellet was resuspended in 50 ml of 5% trichloroacetic acid and stirred for 48 h at 4 °C in the presence of acid-washed glass beads (Sigma-Aldrich). Insoluble material was removed by centrifugation (8,700 × *g*, 15 min), and the supernatant was dialyzed against water at 4 °C. Subsequently, the dialysate was lyophilized, resuspended in 5 ml of H_2O, and centrifuged once more at high speed (25,700 × *g*, 20 min) to remove all residual insoluble material. The supernatant was collected, lyophilized, and stored at room temperature.

Purified Carbohydrates—LTA material from *S. aureus* and *B. subtilis* was purchased from Sigma-Aldrich. The LTA of *L. lactis* subsp. *cremoris* MG1363 was prepared by extraction

with aqueous butanol according to Morath *et al.* (76). The extracellular teichoic acid of *L. monocytogenes* ScottA was purified as described by Brauge *et al.* (77). Extracellular teichoic acid is defined as the TA material embedded in the biofilm matrix, thereby differentiating it from the TA material present in the culture supernatant or in the cell envelope (77). Purification of the CWTAs of the *S. epidermidis* strains 1457 and RP62A and of the *S. aureus* strain MN8m was achieved as described previously by Sadovskaya *et al.* (28) and Vinogradov *et al.* (29), respectively. The cell wall-associated polysaccharide (polysaccharide pellicle), consisting of hexasaccharide repeating units linked via phosphodiester bonds, of MG1363 was purified according to Chapot-Chartier *et al.* (26). Extraction and purification of the individual cell wall-associated carbohydrates (sPS1, sPS2, and CWTA) of Ldb17 was achieved according to Vinogradov *et al.* (27). CWTA was additionally repurified on a BioGel P-2 column.

Monosaccharide Analysis of S. epidermidis 1457 and 5 CWTAs—The CWTA was treated with 48% hydrofluoric acid (4 °C, 24 h), hydrolyzed with 4 M trifluoroacetic acid (120 °C, 2 h), and converted to alditol acetates by conventional methods, thereby avoiding the evaporation to dryness. GC-MS was performed on a Trace GC ULTRA system (Thermo Scientific) equipped with a capillary column (NMTR-5MS; 30 × 0.25 mm) using a temperature gradient of 140 (3 min) to 250 °C at 15 °C/min with a DSQ II MS detector. Control mixtures with equimolar amounts of glycerol, glucose, and *N*-acetylglucosamine were treated in parallel.

Enzyme-coupled Spectrophotometric Assay—The enzymatic activity of GDPD was quantified by measuring the production of Gro3P in a two-step coupled spectrophotometric assay. The GDPD reaction mixture (100 μl) consisted of 50 mM MOPS (pH 7.5); 20 mM $CaCl_2$; recombinantly purified $GDPD_{Ld17}$, $GDPD_{340}$, or derivatives; and a substrate of interest. The final concentration of the substrates used was 2.5 g/liter for the purified carbohydrates and the cell wall-associated carbohydrate extracts and 1 mM for L-α-glycerophosphorylcholine (Sigma-Aldrich). After 30-min incubation at 30 °C, the reaction was stopped by boiling (95 °C, 10 min), and the reaction mixture was cooled to room temperature. Buffer conditions (pH, ionic concentration, and divalent cations) and temperature were adjusted if required to study the relevant GDPD reaction parameters. To evaluate the optimal pH for $GDPD_{Ld17}$ activity, a universal buffer (150 mM KCl, 10 mM KH_2PO_4, 10 mM sodium citrate, and 10 mM boric acid) adjusted to pH values from 4 to 13 was tested. After 30-min incubation with $GDPD_{Ld17}$, the pH of the boiled samples was adjusted to 7 to prevent any influence on the coupled enzymatic reaction.

The amount of Gro3P produced by GDPD was separately measured in a second reaction using Gro3P dehydrogenase, an oxidoreductase that generates NADH in the presence of NAD^+ and Gro3P. A volume of 80 μl of the GDPD reaction was added to the 900 μl of the Gro3P dehydrogenase reaction mixture consisting of 0.8 M hydrazine hydrate buffer (pH 9) supplemented with 0.2 M glycine, 0.5 mM NAD^+, and 10 units/ml Gro3P dehydrogenase. This assay mixture was incubated at 37 °C for 1 h until oxidation of Gro3P was complete. The reduction of NAD^+ to NADH was measured by monitoring the absorbance increase at 340 nm with a spectrophotometer. The GDPD activity is expressed as $\Delta A_{340\ nm}$/(μmol of GDPD × min) with $\Delta A_{340\ nm} = A_{340\ nm}(\text{GDPD}) - A_{340\ nm}(\text{control without GDPD})$. For each substrate, the GDPD concentration was chosen in the linear range of activity.

HPAEC-PAD Analysis—Using the Dionex ICS-3000 system (Sunnyvale, CA), carbohydrate fractions (25 μl) were separated on a CarboPac PA1 analytical exchange column (4 × 250 mm) with a CarboPac PA1 guard column (4 × 50 mm) and an ED40 pulsed electrochemical detector in the PAD mode (all from Dionex Corp.). Elution was performed at a constant flow rate of 1.0 ml/min at 30 °C with eluents A, B, and C consisting of 200 mM NaOH; 100 mM NaOH and 550 mM NaOAc; and Milli-Q water, respectively. The following linear gradient of NaOAc was used with 100 mM NaOH: 0–50 min, 0 mM; 50–51 min, 16 mM; 51–56 min, 100 mM; 56–61 min, 0 mM. CHROMELEON software Version 670 (Dionex Corp.) enabled evaluation of the chromatograms. Enzymatic reactions consisting of 1 μM recombinantly purified GDPD and 2.5 g/liter purified carbohydrates or cell wall-associated carbohydrate extracts were performed at 30 °C for 2 h in a 50 mM MOPS (pH 7.5), 20 mM $CaCl_2$ buffer system. As a positive control for the detection of Gro3P, the aforementioned reaction was performed with 1 mM GPC and 1 μM $GDPD_{Ld17}$. Negative controls used for each HPAEC run were (i) buffer control (50 mM MOPS (pH 7.5), 20 mM $CaCl_2$ buffer), (ii) negative control for the enzyme (50 mM MOPS (pH 7.5), 20 mM $CaCl_2$ buffer plus 1 μM GDPD), (iii) negative control for GPC (50 mM MOPS (pH 7.5), 20 mM $CaCl_2$ buffer plus 1 mM GPC),and (iv) negative control for each carbohydrate (50 mM MOPS (pH 7.5), 20 mM $CaCl_2$ buffer plus the relevant carbohydrate substrate).

NMR Analysis of Ldb17 sPS2 after $GDPD_{Ld17}$ Treatment—Solutions of purified Ldb17 sPS2 (2 g/liter; solution A) and $GDPD_{Ld17}$ (10 μM; solution B) were prepared in a 50 mM MOPS (pH 7.5), 20 mM $CaCl_2$ buffer system. 0.5 ml of solution A and 0.1 ml of solution B were mixed, and the final volume was adjusted to 1 ml with MOPS-$CaCl_2$ buffer (final concentrations, 1 mg/ml purified Ldb17 sPS2 and 1 μM $GDPD_{Ld17}$). In the control experiment, buffer was used instead of $GDPD_{Ld17}$ solution. Reaction mixtures were incubated for 2 h at 30 °C. A 100-μl TCA solution (50%) was added to precipitate the proteins, and the mixtures were fractionated on a Sephadex G-50 column. Elution profiles of two samples were identical, indicating the absence of depolymerization. Fractions corresponding to polysaccharides were collected, lyophilized, repurified on a Sephadex G-50 to remove traces of MOPS, and analyzed by NMR spectroscopy as described in Vinogradov *et al.* (27). In a separate experiment, the phosphate content in the $GDPD_{Ld17}$-treated and untreated sPS2 sample was assessed according to Chen *et al.* (78).

Exohydrolytic Activity of $GDPD_{Ld17}$ on CWTA—The reaction mixture contained 1 ml of purified CWTA (1 g/liter) of *S. epidermidis* strains 1457 and 5 (67), 1 μM $GDPD_{Ld17}$, and 50 mM MOPS (pH 7.5), 20 mM $CaCl_2$ buffer. After incubation for 2 h at 30 °C, the chromatographic profiles of the reaction mixture and the untreated purified CWTAs were analyzed on a Sephadex G-50 gel filtration column as described in Vinogradov *et al.* (27).

Author Contributions—A. C., D. v. S., and J. M. conceived the idea for the project. A. C. conducted most of the experiments, analyzed the results, and wrote the paper. A. C., D. v. S., J. M., I. S., and E. V. were involved in interpretation of the results. E. C. and F. D. B. set up the initial scientific framework for the project. I. S. and E. V. purified the carbohydrates and conducted NMR analysis and Sephadex G-50 gel filtration. J.-P. N. performed mass spectrometry. C. C. and S. B. performed SEC-MALS-RI analysis. C. C. and S. S. created the immuno-EM images. All authors reviewed the results and approved the final version of the manuscript.

Acknowledgments—We thank Prof. M. Loessner and Dr. Y. Shen (Institute of Food, Nutrition and Health, ETH Zurich) for providing purified B. subtilis W23 and 168 teichoic acid.

References

1. Corda, D., Mosca, M. G., Ohshima, N., Grauso, L., Yanaka, N., and Mariggiò, S. (2014) The emerging physiological roles of the glycerophosphodiesterase family. *FEBS J.* **281,** 998–1016
2. Larson, T. J., Ehrmann, M., and Boos, W. (1983) Periplasmic glycerophosphodiester phosphodiesterase of *Escherichia coli*, a new enzyme of the glp regulon. *J. Biol. Chem.* **258,** 5428–5432
3. Tommassen, J., Eiglmeier, K., Cole, S. T., Overduin, P., Larson, T. J., and Boos, W. (1991) Characterization of two genes, glpQ and ugpQ, encoding glycerophosphoryl diester phosphodiesterases of *Escherichia coli*. *Mol. Gen. Genet.* **226,** 321–327
4. Ahrén, I. L., Janson, H., Forsgren, A., and Riesbeck, K. (2001) Protein D expression promotes the adherence and internalization of non-typeable *Haemophilus influenzae* into human monocytic cells. *Microb. Pathog.* **31,** 151–158
5. Cheng, L., Bucciarelli, B., Liu, J., Zinn, K., Miller, S., Patton-Vogt, J., Allan, D., Shen, J., and Vance, C. P. (2011) White lupin cluster root acclimation to phosphorus deficiency and root hair development involve unique glycerophosphodiester phosphodiesterases. *Plant Physiol.* **156,** 1131–1148
6. Cheng, Y., Zhou, W., El Sheery, N. I., Peters, C., Li, M., Wang, X., and Huang, J. (2011) Characterization of the *Arabidopsis* glycerophosphodiesterase (GDPD) family reveals a role of the plastid-localized AtGDPD1 in maintaining cellular phosphate homeostasis under phosphate starvation. *Plant J.* **66,** 781–795
7. Gallazzini, M., Ferraris, J. D., and Burg, M. B. (2008) GDPD5 is a glycerophosphocholine phosphodiesterase that osmotically regulates the osmoprotective organic osmolyte GPC. *Proc. Natl. Acad. Sci. U.S.A.* **105,** 11026–11031
8. Rao, M., and Sockanathan, S. (2005) Transmembrane protein GDE2 induces motor neuron differentiation *in vivo*. *Science* **309,** 2212–2215
9. Wittmann, J., Gartemann, K. H., Eichenlaub, R., and Dreiseikelmann, B. (2011) Genomic and molecular analysis of phage CMP1 from *Clavibacter michiganensis* subspecies *michiganensis*. *Bacteriophage* **1,** 6–14
10. Gill, J. J. (2014) Revised genome sequence of *Staphylococcus aureus* bacteriophage K. *Genome Announc.* **2,** e01173-13
11. Kwan, T., Liu, J., DuBow, M., Gros, P., and Pelletier, J. (2005) The complete genomes and proteomes of 27 *Staphylococcus aureus* bacteriophages. *Proc. Natl. Acad. Sci.* **102,** 5174–5179
12. Vandersteegen, K., Mattheus, W., Ceyssens, P.-J., Bilocq, F., De Vos, D., Pirnay, J. P., Noben, J. P., Merabishvili, M., Lipinska, U., Hermans, K., and Lavigne, R. (2011) Microbiological and molecular assessment of bacteriophage ISP for the control of *Staphylococcus aureus*. *PLoS One* **6,** e24418
13. Gu, J., Liu, X., Lu, R., Li, Y., Song, J., Lei, L., Sun, C., Feng, X., Du, C., Yu, H., Yang, Y., and Han, W. (2012) Complete genome sequence of *Staphylococcus aureus* bacteriophage GH15. *J. Virol.* **86,** 8914–8915
14. Cui, Z., Song, Z., Wang, Y., Zeng, L., Shen, W., Wang, Z., Li, Q., He, P., Qin, J., and Guo, X. (2012) Complete genome sequence of wide-host-range *Staphylococcus aureus* phage JD007. *J. Virol.* **86,** 13880–13881
15. Wang, S., Kong, J., Gao, C., Guo, T., and Liu, X. (2010) Isolation and characterization of a novel virulent phage (phiLdb) of *Lactobacillus delbrueckii*. *Int. J. Food Microbiol.* **137,** 22–27
16. Riipinen, K.-A., Forsman, P., and Alatossava, T. (2011) The genomes and comparative genomics of *Lactobacillus delbrueckii* phages. *Arch. Virol.* **156,** 1217–1233
17. Casey, E., Mahony, J., O'Connell-Motherway, M., Bottacini, F., Cornelissen, A., Neve, H., Heller, K. J., Noben, J. P., Dal Bello, F., and van Sinderen, D. (2014) Molecular characterization of three *Lactobacillus delbrueckii* subsp. *bulgaricus* phages. *Appl. Environ. Microbiol.* **80,** 5623–5635
18. Dupont, K., Janzen, T., Vogensen, F. K., Josephsen, J., and Stuer-Lauridsen, B. (2004) Identification of *Lactococcus lactis* genes required for bacteriophage adsorption. *Appl. Environ. Microbiol.* **70,** 5825–5832
19. Mahony, J., Kot, W., Murphy, J., Ainsworth, S., Neve, H., Hansen, L. H., Heller, K. J., Sørensen, S. J., Hammer, K., Cambillau, C., Vogensen, F. K., and van Sinderen, D. (2013) Investigation of the relationship between lactococcal host cell wall polysaccharide genotype and 936 phage receptor binding protein phylogeny. *Appl. Environ. Microbiol.* **79,** 4385–4392
20. Marchler-Bauer, A., and Bryant, S. H. (2004) CD-search: protein domain annotations on the fly. *Nucleic Acids Res.* **32,** W327–W331
21. Murphy, J., Bottacini, F., Mahony, J., Kelleher, P., Neve, H., Zomer, A., Nauta, A., and van Sinderen, D. (2016) Comparative genomics and functional analysis of the 936 group of lactococcal *Siphoviridae* phages. *Sci. Rep.* **6,** 21345
22. Szklarczyk, R., and Heringa, J. (2004) Tracking repeats using significance and transitivity. *Bioinformatics* **20,** i311–i317
23. Shi, L., Liu, J. F., An, X. M., and Liang, D. C. (2008) Crystal structure of glycerophosphodiester phosphodiesterase (GDPD) from *Thermoanaerobacter tengcongensis*, a metal ion-dependent enzyme: insight into the catalytic mechanism. *Proteins* **72,** 280–288
24. Douillard, F. P., O'Connell-Motherway, M., Cambillau, C., and van Sinderen D. (2011) Expanding the molecular toolbox for *Lactococcus lactis*: construction of an inducible thioredoxin gene fusion expression system. *Microb. Cell Fact.* **10,** 66
25. Swoboda, J. G., Campbell, J., Meredith, T. C., and Walker, S. (2010) Wall teichoic acid function, biosynthesis, and inhibition. *Chembiochem* **11,** 35–45
26. Chapot-Chartier, M.-P., Vinogradov, E., Sadovskaya, I., Andre, G., Mistou, M.-Y., Trieu-Cuot, P., Furlan, S., Bidnenko, E., Courtin, P., Péchoux, C., Hols, P., Dufrêne, Y. F., and Kulakauskas, S. (2010) Cell surface of *Lactococcus lactis* is covered by a protective polysaccharide pellicle. *J. Biol. Chem.* **285,** 10464–10471
27. Vinogradov, E., Sadovskaya, I., Cornelissen, A., and van Sinderen, D. (2015) Structural investigation of cell wall polysaccharides of *Lactobacillus delbrueckii* subsp. *bulgaricus* 17. *Carbohydr. Res.* **413,** 93–99
28. Sadovskaya, I., Vinogradov, E., Li, J., and Jabbouri, S. (2004) Structural elucidation of the extracellular and cell-wall teichoic acids of *Staphylococcus epidermidis* RP62A, a reference biofilm-positive strain. *Carbohydr. Res.* **339,** 1467–1473
29. Vinogradov, ., Sadovskaya, I., Li, J., and Jabbouri, S. (2006) Structural elucidation of the extracellular and cell-wall teichoic acids of *Staphylococcus aureus* MN8m, a biofilm forming strain. *Carbohydr. Res.* **341,** 738–743
30. Karamata, D., Pooley, H. M., and Monod, M. (1987) Expression of heterologous genes for wall teichoic acid in *Bacillus subtilis* 168. *Mol. Gen. Genet.* **207,** 73–81
31. Armstrong, J. J., Baddiley, J., and Buchanan, J. G. (1960) Structure of the ribitol teichoic acid from the walls of *Bacillus subtilis*. *Biochem. J.* **76,** 610–621
32. Larson, T. J., and van Loo-Bhattacharya, A. T. (1988) Purification and characterization of glpQ-encoded glycerophosphodiester phosphodiesterase from *Escherichia coli* K-12. *Arch. Biochem. Biophys.* **260,** 577–584
33. Kusser, W., and Fiedler, F. (1982) Purification, Mr-value and subunit structure of a teichoic acid hydrolase from *Bacillus subtilis*. *FEBS Lett.* **149,** 67–70
34. Kusser, W., and Fiedler, F. (1983) Teichoicase from *Bacillus subtilis* Marburg. *J. Bacteriol.* **155,** 302–310
35. Kusser, W., and Fiedler, F. (1984) A novel glycerophosphodiesterase from *Bacillus pumilus*. *FEBS Lett.* **166,** 301–306
36. Takeda, K., and Uetake, H. (1973) *In vitro* interaction between phage and lipopolysaccharide: a novel glycosidase associated with *Salmonella* phage ϵ15. *Virology* **52,** 148–159

37. Lindberg, A. A., Wollin, R., Gemski, P., and Wohlhieter, J. A. (1978) Interaction between bacteriophage Sf6 and *Shigella flexneri*. *J. Virol.* **27,** 38–44
38. Eriksson, U., Svenson, S. B., Lönngren, J., and Lindberg, A. A. (1979) *Salmonella* phage glycanases: substrate specificity of the phage P22 endorhamnosidase. *J. Gen. Virol.* **43,** 503–511
39. Hughes, K. A., Sutherland, I. W., and Clark, J., and Jones, M. V. (1998) Bacteriophage and associated polysaccharide depolymerases—novel tools for study of bacterial biofilms. *J. Appl. Microbiol.* **85,** 583–590
40. Hanlon, G. W., Denyer, S. P., Olliff, C. J., and Ibrahim, L. J. (2001) Reduction in exopolysaccharide viscosity as an aid to bacteriophage penetration through *Pseudomonas aeruginosa* biofilms. *Appl. Environ. Microbiol.* **67,** 2746–2753
41. Cornelissen, A., Ceyssens, P. J., T'Syen, J., Van Praet, H., Noben, J. P., Shaburova, O. V., Krylov, V. N., Volckaert, G., and Lavigne, R. (2011) The T7-related *Pseudomonas putida* phage φ15 displays virion-associated biofilm degradation properties. *PLoS One* **6,** e18597
42. Hallenbeck, P. C., Vimr, E. R., Yu, F., Bassler, B., and Troy, F. A. (1987) Purification and properties of a bacteriophage-induced endo-*N*-acetylneuramidase specific for poly-α-2,8-sialosyl carbohydrate units. *J. Biol. Chem.* **262,** 3553–3561
43. Stummeyer, K., Dickmanns, A., Mühlenhoff, M., Gerardy-Schahn, R., and Ficner, R. (2005) Crystal structure of the polysialic acid-degrading endosialidase of bacteriophage K1F. *Nat. Struct. Mol. Biol.* **12,** 90–96
44. Stummeyer, K., Schwarzer, D., Claus, H., Vogel, U., Gerardy-Schahn, R., and Mühlenhoff, M. (2006) Evolution of bacteriophages infecting encapsulated bacteria: lessons from *Escherichia coli* K1-specific phages. *Mol. Microbiol.* **60,** 1123–1135
45. Taylor, K. (1965) Enzymatic deacetylation of Vi-polysaccharide by Vi-phage. II. *Biochem. Biophys. Res. Commun.* **20,** 752–756
46. Taylor, K. (1966) Physical and chemical changes of Vi-polysaccharide due to Vi-phage II action. *Acta Biochim. Polon.* **13,** 97–106
47. Caldentey, J., and Bamford, D. H. (1992) The lytic enzyme of the *Pseudomonas* phage f6. Purification sand biochemical characterization. *Biochim. Biophys. Acta* **1159,** 44–50
48. Moak, M., and Molineux, I. J. (2000) Role of the Gp16 lytic transglycosylase motif in bacteriophage T7 virions at the initiation of infection. *Mol. Microbiol.* **37,** 345–355
49. Rydman, P. S., and Bamford, D. H. (2000) Bacteriophage PRD1 DNA entry uses a viral membrane-associated transglycosylase activity. *Mol. Microbiol.* **37,** 356–363
50. Kenny, J. G., McGrath, S., Fitzgerald, G. F., and van Sinderen, D. (2004) Bacteriophage Tuc2009 encodes a tail-associated cell wall-degrading activity. *J. Bacteriol.* **186,** 3480–3491
51. Stockdale, S. R., Mahony, J., Courtin, P., Chapot-Chartier, M. P., van Pijkeren, J. P., Britton, R. A., Neve, H., Heller, K. J., Aideh, B., Vogensen, F. K., and van Sinderen, D. (2013) The lactococcal phages Tuc2009 and TP901–1 incorporate two alternate forms of their tail fiber into their virions for infection specialization. *J. Biol. Chem.* **288,** 5581–5590
52. Zourari, A., Accolas, J. P., and Desmazeaud, M. J. (1992) Metabolism and biochemical characteristics of yogurt bacteria. *Le Lait* **72,** 1–34
53. Munsch-Alatossava, P., Ghafar, A., and Alatossava, T. (2013) Potential of nitrogen gas (N2) flushing to extend the shelf life of cold stored pasteurized milk. *Int. J. Mol. Sci.* **14,** 5668–5685
54. Räisänen, L., Draing, C., Pfitzenmaier, M., Schubert, K., Jaakonsaari, T., von Aulock, S., Hartung, T., and Alatossava, T. (2007) Molecular interaction between lipoteichoic acids and *Lactobacillus delbrueckii* phages depends on D-alanyl and α-glucose substitution of poly(glycerophosphate) backbones. *J. Bacteriol.* **189,** 4135–4140
55. Räisänen, L., Schubert, K., Jaakonsaari, T., and Alatossava, T. (2004) Characterization of lipoteichoic acids as *Lactobacillus delbrueckii* phage receptor components. *J. Bacteriol.* **186,** 5529–5532
56. Ravin, V., Räisänen, L., and Alatossava, T. (2002) A conserved C-terminal region in Gp71 of the small isometric-head phage LL-H and ORF474 of the prolate-head phage JCL1032 is implicated in specificity of adsorption of phage to its host, *Lactobacillus delbrueckii*. *J. Bacteriol.* **184,** 2455–2459
57. Chatterjee, A. N. (1969) Use of bacteriophage-resistant mutants to study the nature of the bacteriophage receptor site of *Staphylococcus aureus*. *J. Bacteriol.* **98,** 519–527
58. Coyette, J., and Ghuysen, J.-M. (1968) Structure of the cell wall *Staphylococcus aureus*, strain Copenhagen. IX. Teichoic acid and phage adsorption. *Biochemistry* **7,** 2385–2389
59. Archibald, A. R. (1976) Cell wall assembly in *Bacillus subtilis.* Development of bacteriophage binding properties as a result of the pulsed incorporation of teichoic acids. *J. Bacteriol.* **127,** 956–960
60. Givan, A. L., Glassey, K., Green, R. S., Lang, W. K., Anderson, A. J., and Archibald, A. R. (1982) Relation between wall teichoic acid content of *Bacillus subtilis* and efficiency of adsorption of bacteriophages SP50 and 425. *Arch. Microbiol.* **133,** 318–322
61. Baptista, C., Santos, M. A., and São-José, C. (2008) Phage SPP1 Reversible adsorption to *Bacillus subtilis* cell wall teichoic acids accelerates virus recognition of membrane receptor YueB. *J. Bacteriol.* **190,** 4989–4996
62. Eugster, M. R., and Loessner, M. J. (2012) Wall teichoic acids restrict access of bacteriophage endolysin Ply118, Ply511, and PlyP40 cell wall binding domains to the *Listeria monocytogenes* peptidoglycan. *J. Bacteriol.* **194,** 6498–6506
63. Wendlinger, G., Loessner, M. J., and Scherer, S. (1996) Bacteriophage receptors on *Listeria monocytogenes* cells are the *N*-acetylglucosamine and rhamnose substituents of teichoic acids or the peptidoglycan itself. *Microbiology* **142,** 985–992
64. Munsch-Alatossava, P., and Alatossava, T. (2013) The extracellular phage-host interactions involved in the bacteriophage LL-H infection of *Lactobacillus delbrueckii* ssp. *lactis* ATCC 15808. *Front. Microbiol.* **4,** 408
65. Rousseau, G. M., and Moineau, S. (2009) Evolution of *Lactococcus lactis* phages within a cheese factory. *Appl. Environ. Microbiol.* **75,** 5336–5344
66. Castro-Nallar, E., Chen, H., Gladman, S., Moore, S. C., Seemann, T., Powell, I. B., Hillier, A., Crandall, K. A., and Chandry, P. S. (2012) Population genomics and phylogeography of an Australian dairy factory derived lytic bacteriophage. *Genome Biol. Evol.* **4,** 382–393
67. Sadovskaya, I., Chaignon, P., Kogan, G., Chokr, A., Vinogradov, E., and Jabbouri, S. (2006) Carbohydrate-containing components of biofilms produced *in vitro* by some staphylococcal strains related to orthopaedic prosthesis infections. *FEMS Immunol. Med. Microbiol.* **47,** 75–82
68. Kornspan, J. D., and Rottem, S. (2012) Phospholipase A and glycerophosphodiesterase activities in the cell membrane of *Mycoplasma hyorhinis*. *FEMS Microbiol. Lett.* **332,** 34–39
69. Simocková, M., Holic, R., Tahotná, D., Patton-Vogt, J., and Griac P. (2008) Yeast Pgc1p (YPL206c) controls the amount of phosphatidylglycerol via a phospholipase C-type degradation mechanism. *J. Biol. Chem.* **283,** 17107–17115
70. Sundaralingam, M., and Jensen, L. H. (1965) Crystal and molecular structure of a phospholipid component: L-α-glycerophosphorylcholine cadmium chloride trihydrate. *Science* **150,** 1035–1036
71. Laemmli, U. K. (1970) Cleavage of structural proteins during the assembly of the head of bacteriophage T4. *Nature* **227,** 680–685
72. Lavigne, R., Noben, J.-P., Hertveldt, K., Ceyssens, P.-J., Briers, Y., Dumont, D., Roucourt, B., Krylov, V. N., Mesyanzhinov, V. V., Robben, J., and Volckaert, G. (2006) The structural proteome of *Pseudomonas* bacteriophage φKMV. *Microbiology* **152,** 529–534
73. Sambrook, J., and Russell, D. W. (2001) *Molecular Cloning: A Laboratory Manual*, 2nd Ed., pp. A8.40–18.51, Cold Spring Harbor Laboratory Press, Cold Spring Harbor, NY
74. Bradford, M. M. (1976) A rapid and sensitive method for the quantitation of microgram quantities of protein utilizing the principle of protein-dye binding. *Anal. Biochem.* **72,** 248–254
75. Sciara, G., Blangy, S., Siponen, M., Mc Grath, S., van Sinderen, D., Tegoni, M., Cambillau, C., and Campanacci, V. (2008) A topological model of the baseplate of lactococcal phage Tuc2009. *J. Biol. Chem.* **283,** 2716–2723
76. Morath, S., Geyer, A., and Hartung, T. (2001) Structure-function relationship of cytokine induction by lipoteichoic acid from *Staphylococcus aureus*. *J. Exp. Med.* **193,** 393–397
77. Brauge, T., Sadovskaya, I., Faille, C., Benezech, T., Maes, E., Guerardel, Y., and Midelet-Bourdin, G. (2016) Teichoic acid is the major polysaccharide present in the *Listeria monocytogenes* biofilm matrix. *FEMS Microbiol. Lett.* **363,** fnv229
78. Chen, P. S., Toribara, T. Y., and Warner, H. (1956) Microdetermination of phosphorus. *Anal. Chem.* **28,** 756–758